

iScience, Volume 24

Supplemental information

A high-performance triboelectric-electromagnetic hybrid wind energy harvester based on rotational tapered rollers aiming at outdoor IoT applications

Yan Fang, Tianyi Tang, Yunfei Li, Cheng Hou, Feng Wen, Zhan Yang, Tao Chen, Lining Sun, Huicong Liu, and Chengkuo Lee

Supporting Information for

A high-performance triboelectric–electromagnetic hybrid wind energy harvester based on rotational tapered rollers aiming at outdoor IoT applications

Yan Fang^{1,6}, Tianyi Tang^{1,6}, Yunfei Li^{2,6}, Cheng Hou¹, Feng Wen^{3,4,5}, Zhan Yang^{1,*},
Tao Chen¹, Lining Sun¹, Huicong Liu^{1,7,*}, and Chengkuo Lee^{3,4,5,*}

¹School of Mechanical and Electric Engineering, Jiangsu Provincial Key Laboratory of Advanced Robotics, Soochow University, Suzhou 215123, China

²State Key Laboratory of Robotics and System, Harbin Institute of Technology (HIT), Harbin 150001, China

³Department of Electrical & Computer Engineering, National University of Singapore, 4 Engineering Drive 3, Singapore, 117576, Singapore

⁴National University of Singapore Suzhou Research Institute (NUSRI), Suzhou Industrial Park, Suzhou, 215123, China

⁵Center for Intelligent Sensors and MEMS, National University of Singapore, E6 #05-11F, 5 Engineering Drive 1, Singapore, 117608, Singapore

⁶These authors contribute equally to this work.

⁷Lead contact

* Correspondence: hcliu078@suda.edu.cn (H.L.), yangzhan@suda.edu.cn (Z.Y.), elelc@nus.edu.sg (C.L.)

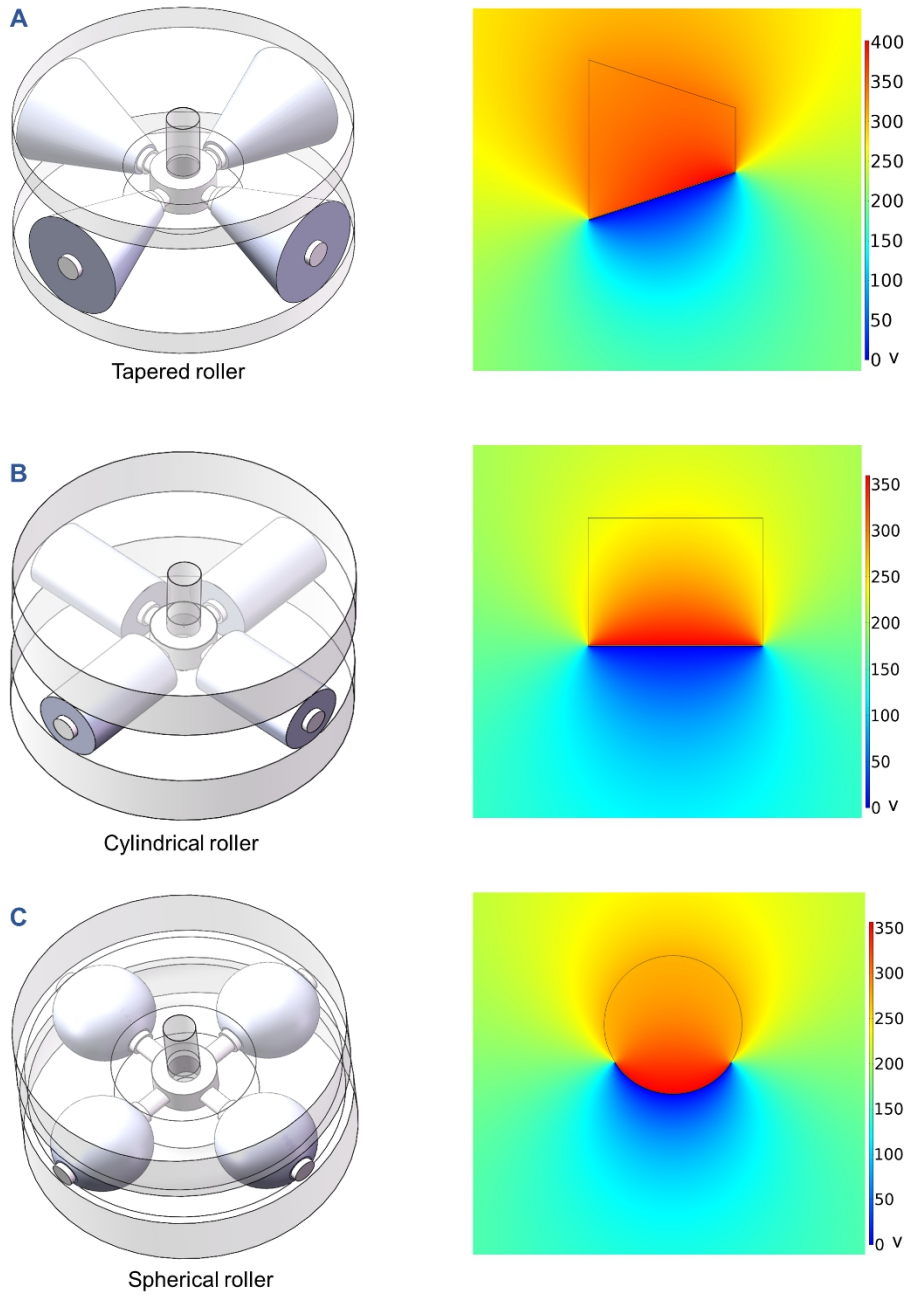


Figure S1. The potential distribution between the electrodes of TENG with different roller shapes, Related to Figure 1.

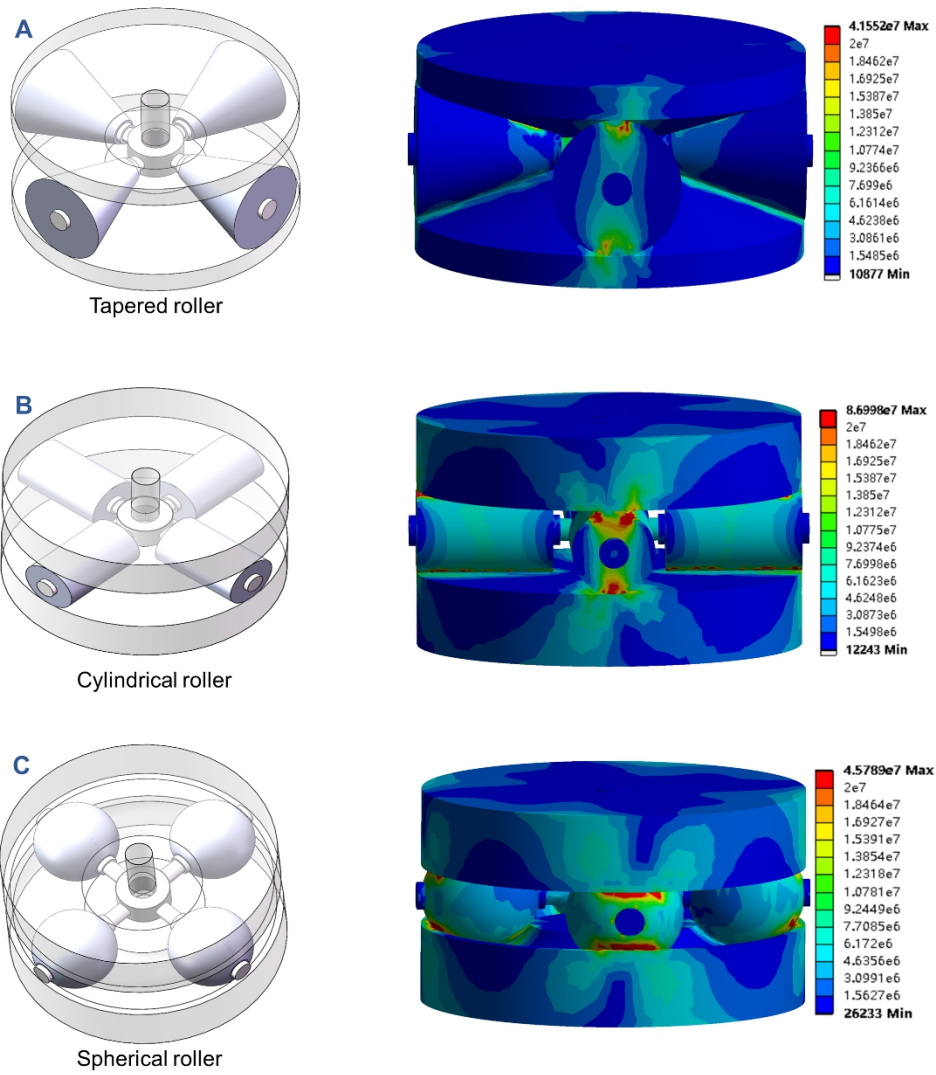


Figure S2. The distribution of equivalent stress of different roller shapes, Related to Figure 1.

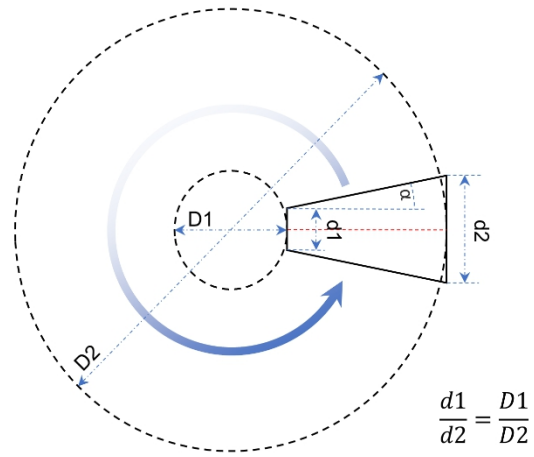


Figure S3. The design parameters of the tapered roller, Related to Figure 1.

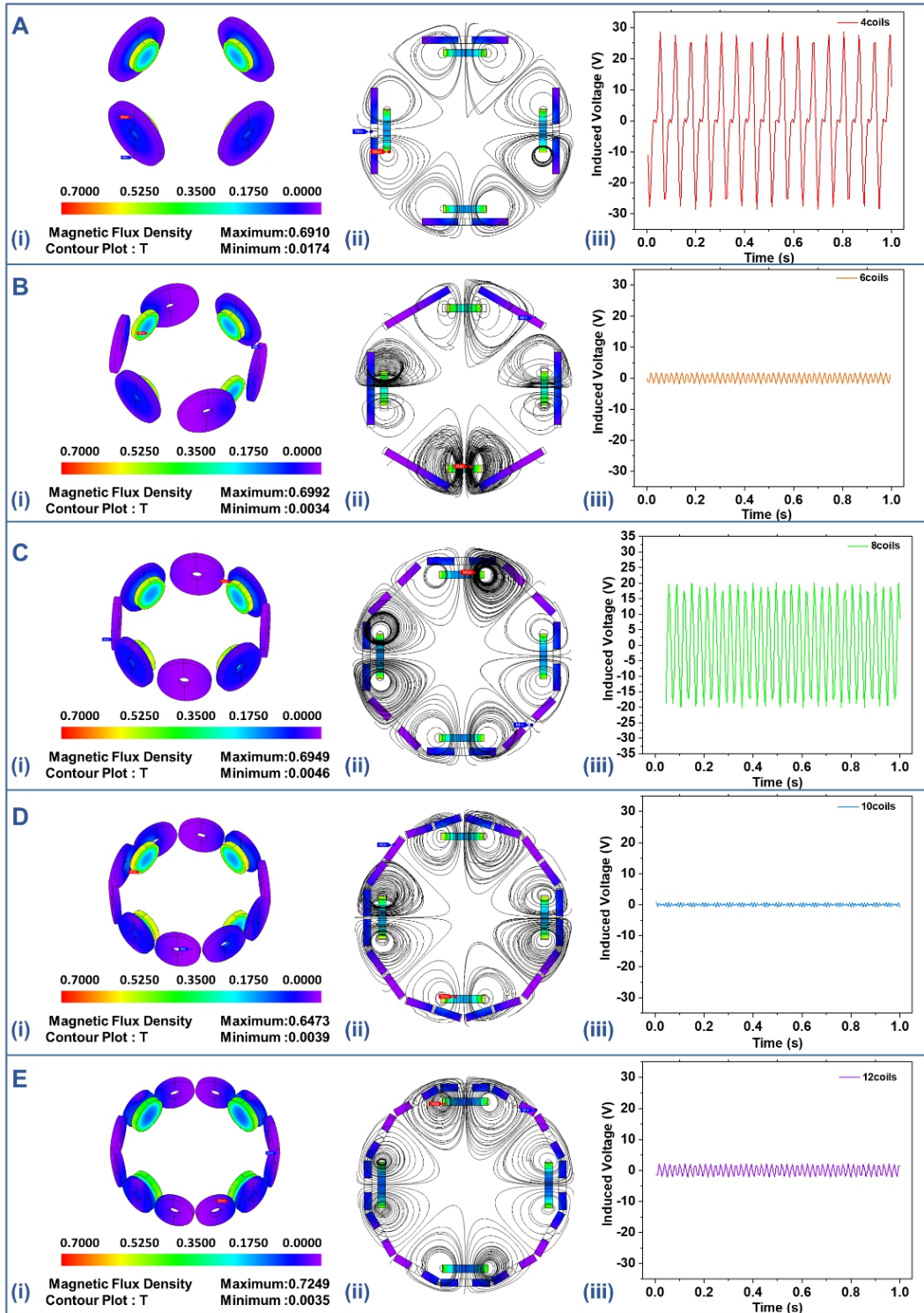


Figure S4. Numerical calculation results of the EMG with different numbers of coils, Related to Figure 2.

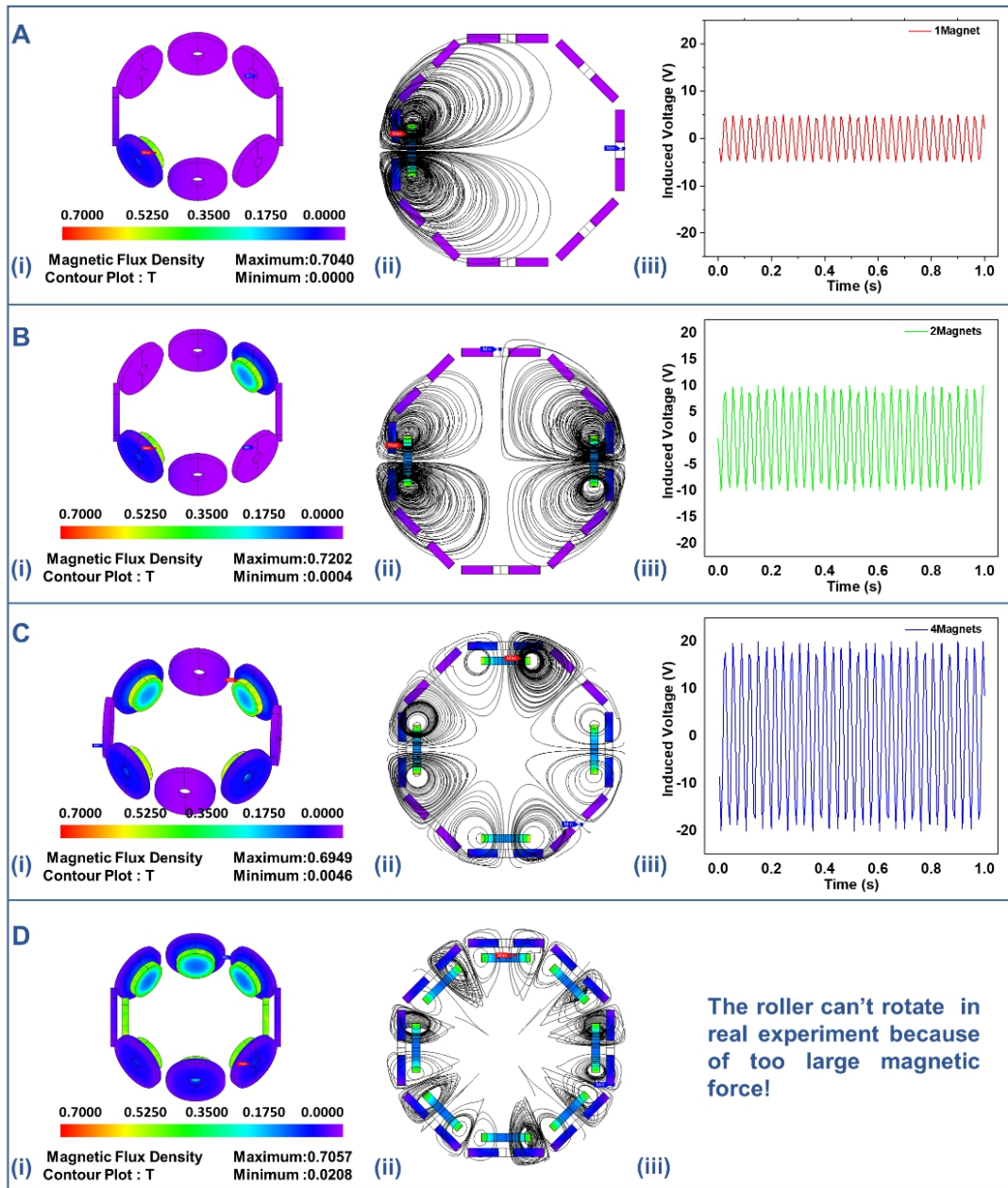


Figure S5. Numerical calculation results of the EMG with different numbers of magnets, Related to Figure 2.

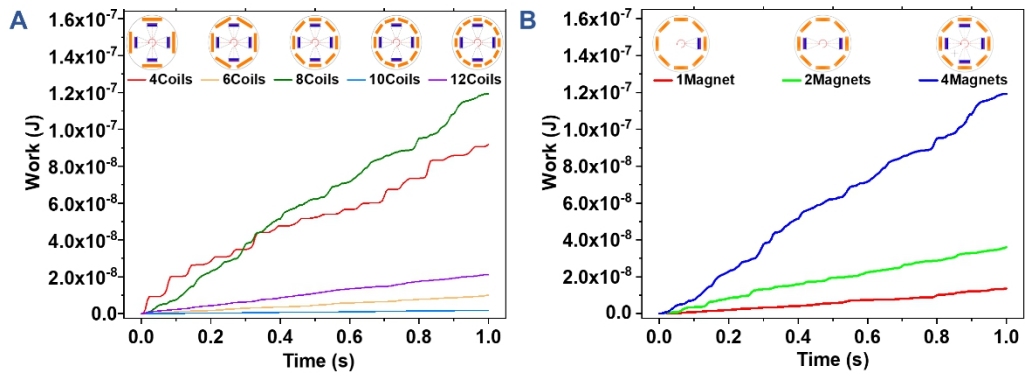


Figure S6. The numerical calculation results of average output power with different numbers of coils and different numbers of magnets, Related to Figure 2.

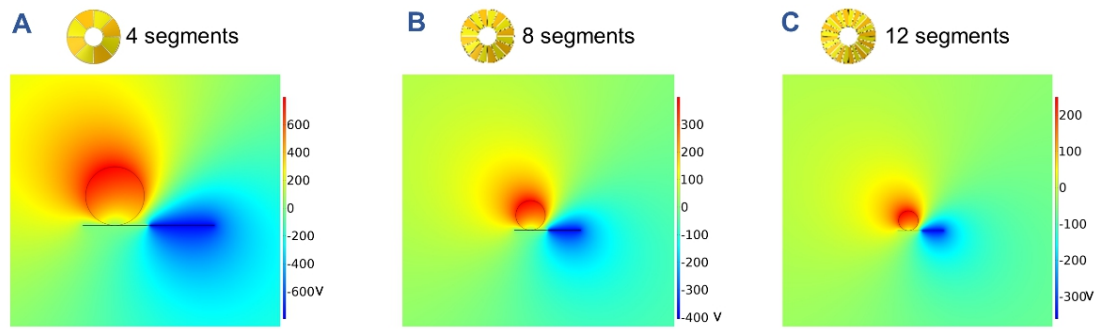
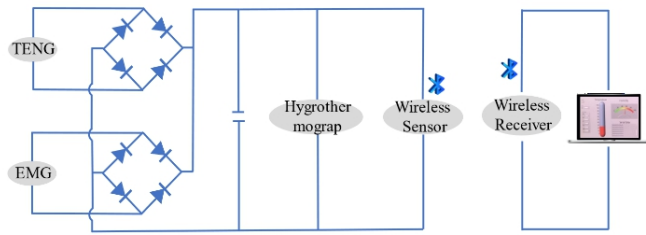
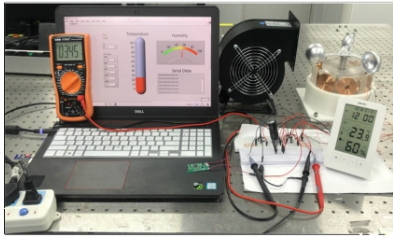


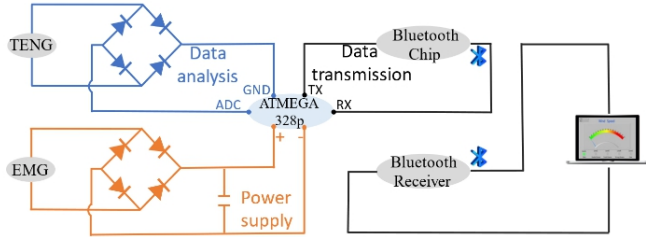
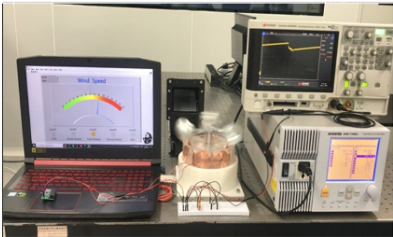
Figure S7. The potential distribution of the TENG with different size of tapered rollers and different segments of electrodes, Related to Figure 3.

A



Self-powered wireless temperature and humidity sensing node

B



Self-powered wireless anemograph

Figure S8. The power management circuit diagram, Related to Figure 6.